Inorganic Chemistry
Cite This: Inorg. Chem. 2019, 58, 14777−14789
Article
pubs.acs.org/IC

Pushing 3c−4e Bonds to the Limit: A Coupled Cluster Study of Stepwise Fluorination of First-Row Atoms

Vytor P. Oliveira,[†] Elfi Kraka,[‡] and Francisco B. C. Machado*[,†]

[†]Instituto Tecnológico de Aeronáutica (ITA), Departamento de Química, São José dos Campos, 12228-900 São Paulo, Brazil
[‡]Department of Chemistry, Southern Methodist University, 3215 Daniel Avenue, Dallas, Texas 75275-0314, United States

Supporting Information

ABSTRACT: To better understand why hypervalent F, O, N, C, and B compounds are rarely stable, we carried out a systematic study of 28 systems, including anionic, cationic, and neutral molecules, held together by covalent, hypervalent, and noncovalent bonds. Molecular geometries, frequencies, atomic charges, electrostatic potentials, energy and electron densities, Mayer bond orders, local stretching force constants, and bond strength orders (BSOs) were derived from high accuracy CCSD(T) calculations and utilized to compare the strength and nature of hypervalent bonds with other types of bonds. All hypervalent molecules studied in this work were found to be either first-order transition states or unstable to dissociation, with F_3^- and OF_3^- as the only exceptions. For several systems, we found that a weak noncovalent bonded complex is more stable than a hypervalent one, due to the high energetic cost to accommodate an extra ligand, which can surpass the stability gained by 3c−4e bonding.

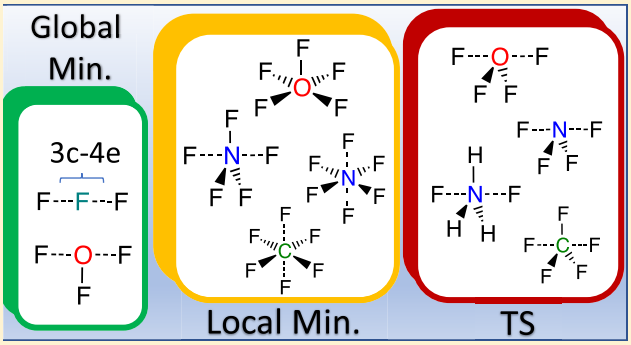

INTRODUCTION

There are significant differences between the chemistry of first row main elements and the heavier main elements.[1,2] Perhaps the most remarkable ones are (i) the capability of first row elements to form π double bonds and triple bonds of comparable strength to σ bonds[3] and (ii) that they are unlikely to form hypervalent species. The strong π bonds formed by first row elements are attribute to sp^n (n = 1, 2) hybridization, which is more effective for first row atoms due to the similar extension of their 2s and 2p valence orbitals.[4] The unlikeliness of first row elements to form stable hypervalent species is not fully understood yet, so far being attributed to the small size of these elements,[5,6] low polarizability, and/or high first and second ionization potentials.[7]

Even though there is a limited number of experimentally observed hypervalent/hypercoordinate first row molecules,[8−15] and few others predicted to be stable on the basis of theoretical studies but not observed yet,[16−21] these molecules may have a great impact in chemistry. Their unusual electronic structure might not only enrich our fundamental understanding of the chemical bond, providing a connection between noncovalent and covalent bonding,[22−25] but could also have important practical implications, such as in material science, on the design of fluorinating agents,[26] nanowires,[18] two-dimensional materials,[17,27,28] and supramolecular fluoride receptors.[13] Not only stable molecules but also unstable first-order TS involving hypervalent first row molecules are of interest. The best example is the commonly found pentacoordinated carbon in the transition state (TS) of bimolecular substitution reactions (S_N2).[29−31] A better understanding of the bonding mechanism in these TS structures could help to improve the selectivity and/or to reduce the activation energy of these reactions.

The term hypervalent was coined by Musher[32] to describe all molecules and ions formed by elements from groups 15−18 of the periodic table that cannot be described by a single Lewis representation without violating the valence octet rule,[33] i.e., more than four electron pairs are assigned to the center atom. An early hypothesis for the bonding mechanism in hypervalent molecules[34,35] suggested an extension of the octet rule via the formation of hybrid sp^md^n orbitals. However, this hypothesis could not be conciliated with (i) the high energy required to promote electrons to the lowest empty d orbital of main elements, such as for P and S; (ii) the incompatible extension of the d orbital compared to valence s and p orbitals of main elements; and (iii) the low occupancy of d orbitals observed in several different hypervalent molecules (for a detailed discussion see refs 36−38).

A well accepted and frequently used alternative explanation for bonding in electron-rich hypervalent molecules excluding d-orbital participation was provided by Musher[32] based on the Rundle−Pimentel three-center four-electron (3c−4e) molecular orbital (MO) bond model.[39,40] Taking F_3^- as an example, the linear combination of the p_z orbitals of the three linearly aligned F atoms leads to a set of three molecular orbitals, i.e., a totally bonding, a nonbonding, and an antibonding orbital.

Received: August 13, 2019
Published: October 24, 2019

DOI: 10.1021/acs.inorgchem.9b02458
Inorg. Chem. 2019, 58, 14777−14789

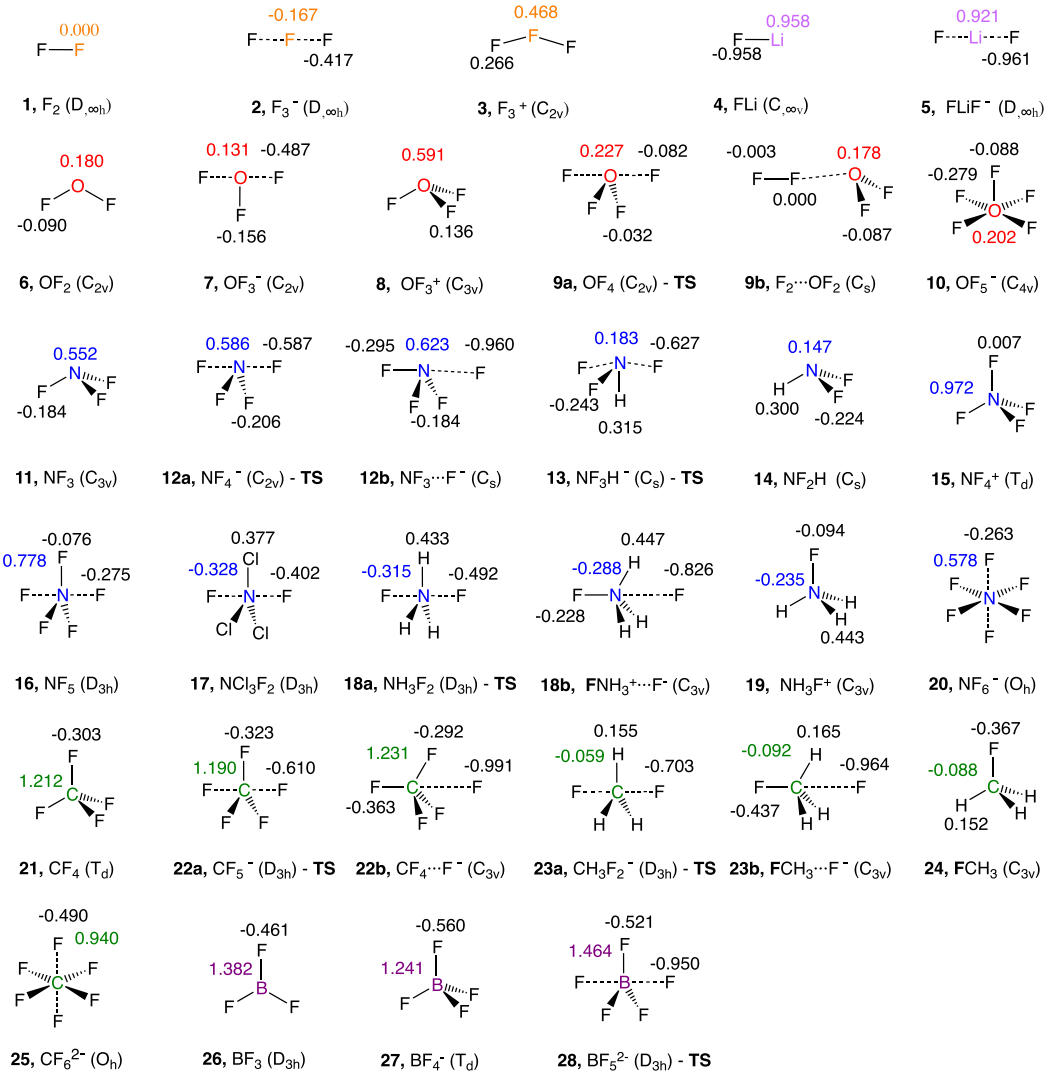

Figure 1. Schematic presentation of the geometries of complexes **1**−**28** with selected color coded NPA atomic charges obtained from CCSD(T)/aug-cc-pVTZ response density.

Only the bonding and nonbonding orbitals are occupied, leading to a fractional bond order of 0.5 for each FF bond. The combination of p_x and p_y valence orbitals leads to two analog sets of three π molecular orbitals, but in this case, all of them are occupied. Therefore, there is no π-bonding contribution. This model does not imply an extension of the octet at the center atom, since the exceeding two electrons are assigned to a nonbonding orbital located at the ligands. Recent studies[41,42] based on X-ray diffraction data and theoretical calculations have attributed eight or less valence electrons to the central atom of SO_4^{2-} and PO_4^{3-}. The polarity of the SO and PO were considered to be essential for the nonextension of the octet of S and P. Munzarová and Hoffmann showed that the Rundle−Pimental model can be improved by considering s,p orbital mixing.[43]

An equivalent explanation based on the valence bond (VB) resonance model was given by Coulson[35] for the hypervalent bond in XeF_2. Out of six VB structures found, the resonance between $F^-\cdots{}^+XeF$ and $FXe^+\cdots F^-$ was considered to play the most important role in stabilizing XeF_2. In contrast, the charge-shift bonding model attributes the stabilization of 3c−4e bonding not to the sum of individual VB structure contributions but to the resonance energy that arises from the mixing of ionic and covalent structures.[38,44] Another VB model, the recoupled-pair bond model,[45,46] describes hypervalent bond formation as a two-step process. In the first step, a lone pair of the center atom is decoupled into a biradical. In the second step, these two electrons can recouple with an electron from one ligand forming a recoupled pair bond (a weak 2c−3e bond) or two ligands in a recoupled pair dyad (analog to the 3c−4e bond). The balance between the energetic cost associated with the decoupling and the energetic gain with the recoupling process is used to explain why hypervalent bonds are mostly observed for center atoms of the second and later rows combined with electronegative ligands but rarely found for first-row center atoms. Steric constraints are also considered to play a major role. For example, according to Bickelhaupt and co-workers' ball-in-a-box model,[6,31] the D_{3h} hypervalent $(Cl{-}SiH_3{-}Cl)^-$ is stable because Si fits perfectly inside the box determined by the mutual steric repulsion between Cl and H ligands, whereas C is too small and cannot bind well to all five ligands simultaneously. Thus, hypervalent $(Cl{-}CH_3{-}Cl)^-$ deforms into the noncovalent $ClCH_3\cdots Cl^-$ complex to gain stability. Landrum et al.[22] utilized the Rundle−Pimentel 3c−4e bond model and a donor−acceptor model to trace a connection

DOI: 10.1021/acs.inorgchem.9b02458
Inorg. Chem. 2019, 58, 14777−14789

between hypervalent bonds and strong hydrogen bonds. Recent studies do also propose a connection between hypervalent bonds and halogen[23−25] or tetrel bonds.[6,47]

Theoretical studies of first-row hypervalent molecules have usually been restricted (but not limited[48]) to the analysis of geometric parameters,[6,30,49,50] chemical shifts,[8] atomic charges and natural bond orbitals (NBOs),[37,51−53] dissociation energies and their decomposition into model dependent terms,[6,21,22,29,49,54,55] and topological analysis of the electron density.[51,56] These studies predominantly focused on the analysis of a limited number of similar systems, (e.g., pentacoordinate carbon or boron) or on explaining the energetic barrier of S_N2 reactions involving pentacoordinate carbon,[6,29,30,48,54,57] investigating the viability of new molecules[11,16,20,21,49,50] such as NF_5 and NF_6^-, or verifying the existence of hypervalent bonds based on interatomic distance or topological parameter at the density critical point of a bond.[8,11,51,53,56] However, so far, a systematic study on the strength of hypervalent bonds in the series F, O, N, C, and B considering ionic and neutral hyperfluorinated molecules is still missing. Such a study could provide for the first time a general explanation for the low stability of 3c−4e hypervalent bonds in first-row elements and improve our understanding of the relationship between noncovalent and hypervalent bonds.

To fill this gap, we combined state of the art coupled cluster calculations with a bond strength analysis based on vibrational spectroscopy. As discussed in previous papers,[58−60] the local mode force constant of a stretching vibration provides a unique way to probe the strength of a bond without breaking it (i.e., the electronic structure is preserved). Normal mode force constants derived from normal vibrational modes are not suitable for this purpose due to their delocalized nature, caused by mode coupling.[61,62] To solve this problem Konkoli and Cremer[63] solved a mass-decoupled analog of the Wilson equation, leading to local vibrational modes free of mass and electronic coupling. The local stretching force constant k^a(AB) associated with a bond AB provides an ideal measure of its intrinsic strength, successfully employed so far in more than 35 papers involving covalent, noncovalent bonds (see refs 64 and 65 and references therein), and hypervalent bonded systems.[24]

In the present study, local stretching force constants were utilized to assess the intrinsic bond strength of hypervalent bonding. The quantitative analysis of the hypervalent bond strength was complemented by the analysis of reaction energetics, atomic charges, and topological parameters of the electron and energy density, to provide an answer for the following questions:

(i) Are there any experimentally observable hyperfluorinated first row molecules besides F_3^-?

(ii) What parameters can we use to distinguish hypervalent first-row molecules from hypercoordinate molecules (molecules in which the extra contacts are due to noncovalent interactions)?

(iii) How strong can a hypervalent bond involving first-row atoms be compared to covalent and noncovalent bonds?

(iv) What is the nature of these hypervalent bonds? Is there any similarity to a covalent bond?

(v) What strategy can be applied to obtain hypercoordinate C, N, O compounds?

To make the distinction between hypervalent and hypercoordinated molecules[66] as simple as possible, we will use in the following the term hypervalent whenever 3c−4e bonds are well characterized in terms of geometry, orbital analysis, bond strength, and topological parameters of the electron density, whereas the term hypercoordinated will be used to denote noncovalently bonded complexes.

COMPUTATIONAL METHODS

The geometries of molecules **1**−**28** (shown in Figure 1) were fully optimized at the coupled cluster level utilizing CCSD(T)[67] (all-order single, double, and perturbative triple excitations are included). A frozen-core approximation was used in all calculations; i.e., 1s core−electrons of B, C, N, O, and F and 1s, 2s, 2p core electrons of Cl were kept uncorrelated. This method was combined with Dunning augmented triple-ζ basis set aug-cc-pVTZ,[68−70] which contains diffuse basis functions to describe the charge distribution of anions and dispersion in noncovalent interactions. A negative vertical detachment energy (VDE) may arise due to an insufficient set of diffuse functions.[71] Therefore, the VDE of anionic systems was calculated (see Table S1 in the Support Information (SI)). All values were found to be positive, confirming the suitability of the diffuse set of aug-cc-pVTZ used for the present study.

The perturbative triple excitations are found to be essential for a quantitative and even qualitative comparison of second-order properties of systems, in which electron pairs are clustered in a confined space of the molecule, e.g., when a system contains two or more adjacent electronegative elements such as F, O, and N.[72] This trend becomes evident in the hyper-fluorinated anion series F_3^- ($D_{\infty h}$), OF_3^- (C_{2v}), NF_4^- (C_{2v}), and CF_5^- (D_{3h}; see Table S2). Although CCSD bond distances deviate by less than 3%, k^a values deviate by as much as 73% compared to CCSD(T) results (see also ref 73). As expected, the mean absolute deviation of k^a values of XF bonds of each of these molecules decreases with the electronegativity of X (X = F > O > N > C). An imaginary frequency of 197i cm^{-1} is observed for OF_3^- (C_{2v}) at the CCSD level, but at the CCSD(T) level all frequencies of this molecule are real.

Each stationary point obtained via geometry optimization was identified as either a minimum or a first-order TS (molecules **9a**, **12a**, **13**, **18a**, **22a**, **23a**, and **28**) with the help of the analytical harmonic vibrational frequencies computed at the same level as used for geometry optimization.[74] Local vibrational modes were then obtained following the procedure described by Konkoli and Cremer.[63] Each local mode is related to a single normal mode via an adiabatic connection scheme[75] providing a direct connection to the normal modes and a physically meaningful way to decompose normal modes into local modes and *vice versa*.[75−77] The analysis of the bond strength can be simplified by transforming local stretching force constants into relative bond strength orders (BSO)[78] based on a generalization of the Badger rule[79−81] proposed by Kraka et al.[78] According to the generalized Badger rule, BSO values are related to k^a values via a power relationship BSO $n = a(k^a)^b$, where constants $a = 0.418$ and $b = 0.564$ were defined in this work via the 2c−2e FF single bond in F_2 with $n = 1.00$ and the corresponding 3c−4e bond in F···F···F^- with $n = 0.50$.

An inspection of potential multireference character of molecules **1**−**28** based on the occupancy of natural orbitals (Figures S1−S5 in the SI), T1 diagnostic,[82] and the magnitude of the largest T2 amplitude (Table S5 in the SI) showed that a few of them had potential multireference characters (T1 diagnostic > 0.02 or T2 largest amplitude > 0.1). Moderate cases (where T2 largest amplitude < 0.2) are F_2, F_3^-, F_3^+, OF_3^-, and NF_4^-. Molecules F_2, F_3^-, and F_3^+ are well-known to possess an RHF → UHF instability of the wave function, which can be solved by employing the Brueckner reference (*B*).[83,84] This also seems to be the case for other molecules such as OF_3^- and NF_4^-. Since few changes were observed in the geometries and k^a values of these molecules going from RHF-CCSD(T) to B-CCD(T) (see Table S5 in the SI), all results discussed in this work are based on RHF wave function results. A more critical multireference character was found for OF_4 and OF_5^- (both molecules had a fractional occupation of the lowest unoccupied natural orbital of 0.4, Figure S2). OF_4 is a TS with very long OF axial bonds. Several other geometries were tested but no minimum energy geometry was found

DOI: 10.1021/acs.inorgchem.9b02458
Inorg. Chem. 2019, 58, 14777−14789

Table 1. Geometry, Topological Parameters, and Vibrational Data for All Molecules Studied[a]

#	molecule (sym.)	bond	r	ρ_b	H_b	$\nabla^2\rho_b$	k^a	BSO	MBO	ω^a	$\omega^\mu(\#;\omega^a\%)$
					fluorine and lithium derivatives						
1	$[F_2]$ $(D_{\infty h})$	FF	1.418	0.277	−0.176	0.514	4.700	1.000	0.8	916	916(1; 100%)
2	$[F_3^-]$ $(D_{\infty h})$	FF	1.739	0.113	−0.027	0.449	1.376	0.500	0.4	496	398(3; 39%) 548(4;61%)
3	$[F_3^+]$ (C_{2v})	FF	1.435	0.261	−0.160	0.589	3.201	0.805	0.7	756	722(2; 63%) 822(3; 36%)
4	[FLi] $(C_{\infty h})$	FLi	1.590	0.072	0.016	0.691	2.366	0.679	0.8	885	885(1; 100%)
5	$[FLiF^-]$ $(D_{\infty h})$	FLi	1.707	0.051	0.015	0.458	1.374	0.500	0.7	675	575(3; 46%) 727(4; 54%)
					oxygen derivatives						
6	$[OF_2]$ (C_{2v})	OF	1.412	0.295	−0.202	0.328	3.987	0.911	0.8	883	859(2; 59%) 945(3; 37%)
7	OF_3^- (C_{2v})	(OF)eq	1.436	0.273	−0.178	0.349	3.306	0.820	0.8	804	184(1; 11%) 851(6; 89%)
		(OF)ax	1.767	0.114	−0.030	0.384	0.933	0.402	0.4	427	280(2; 27%) 406(4; 26%) 502(5; 47%)
8	OF_3^+ (C_{3v})	OF	1.398	0.313	−0.212	0.427	2.985	0.774	0.8	764	770(4; 72%) 864(6; 18%)
9a	OF_4 (C_{2v})[TS]	(OF)eq	1.392	0.314	−0.222	0.325	3.989	0.912	0.8	883	884(8; 56%) 921(9; 39%)
		(OF)ax	2.602	0.011	0.004	0.066	0.082	0.102	0.0	127	189i(1; 54%) 77(5; 12%) 134(6; 33%)
9b	$F_2\cdots OF_2$ (C_s)	FF	1.419	0.276	−0.175	0.514	4.663	0.996	0.8	913	913(8; 100%)
		(OF)[b]	2.750	0.007	0.003	0.044	0.040	0.068	0.0	88	54(4; 10%) 80(5; 89%)
		OF	1.412	0.295	−0.202	0.328	3.979	0.910	0.8	882	859(7; 59%) 945(9; 37%)
10	OF_5^- (C_{4v})	(OF)ax	1.431	0.280	−0.181	0.363	3.075	0.787	0.8	775	802(12; 93%)
		(OF)eq	1.866	0.090	−0.016	0.342	0.406	0.251	0.3	282	140(2; 46%) 267(9; 13%) 463(10; 24%)
					nitrogen derivatives						
11	$[NF_3]$ (C_{3v})	NF	1.375	0.330	−0.338	−0.352	3.945	0.906	0.9	911	924(4; 70%) 1045(6; 17%)
12a	NF_4^- (C_{2v}) [TS]	(NF)eq	1.369	0.332	−0.348	−0.394	3.560	0.855	0.9	866	883(8; 53%) 991(9; 30%)
		(NF)ax	1.818	0.108	−0.028	0.290	0.895	0.392	0.5	434	80i(1; 98%)
12b	$NF_3\cdots F^-$ (C_s)	(NF)ax	1.469	0.257	−0.203	−0.004	1.627	0.550	0.8	585	144(3; 17%) 474(4; 24%) 624(6; 19%) 725(7; 40%)
		(NF)[b]	2.422	0.024	0.003	0.105	0.145	0.140	0.1	175	126(1; 10%)144(3; 87%)
		(NF)eq	1.362	0.340	−0.362	−0.427	3.705	0.874	1.0	883	929(8; 50%) 1030(9; 28%)
13	NF_3H^- (C_s) [TS]	(NF)eq	1.392	0.304	−0.309	−0.308	3.706	0.875	0.9	883	922(6; 91%)
		(NH)eq	1.016	0.365	−0.634	−2.323	6.886	1.240	0.9	3526	3551(9; 99%)
		(NF)ax	1.828	0.099	−0.024	0.287	1.157	0.453	0.4	494	400i(1; 70%) 395(4; 23%)
14	$[NF_2H]$ (C_s)	NF	1.400	0.300	−0.296	−0.267	4.102	0.926	0.9	929	910(2; 59%) 992(3; 37%
		NH	1.027	0.356	−0.563	−2.029	6.272	1.177	0.9	3365	3368(6; 100%)
15	$[NF_4^+]$ (T_d)	NF	1.311	0.405	−0.452	−0.543	5.581	1.102	1.1	1084	611(3; 11%) 859(6; 17%) 1186(7; 71%)
16	NF_5 (D_{3h})	(NF)eq	1.382	0.332	−0.308	−0.189	2.533	0.706	0.9	730	204(1; 20%) 396(3; 14%) 541(5; 14%) 680(9; 11%) 998(11; 41%)
		(NF)ax	1.578	0.208	−0.122	0.162	1.355	0.496	0.7	534	396(3; 27%) 519(4; 57%) 775(10; 12%)
17	NCl_3F_2 (D_{3h})	(NCl) eq	1.745	0.202	−0.148	−0.155	2.442	0.691	0.8	642	284(3; 18%) 360(7; 10%) 459(10; 12%) 795(11; 57%)
		(NF)ax	1.759	0.128	−0.043	0.271	0.614	0.317	0.5	359	284(3; 21%) 326(6; 40%) 417(9; 34%)
18a	NH_3F_2 (D_{3h}) [TS]	(NH)eq	1.007	0.357	−0.670	−2.493	7.443	1.296	0.9	3666	3533(10; 33%) 3740(11; 66%)
		(NF)ax	1.720	0.132	−0.049	0.296	2.277	0.664	0.5	692	419i(1; 79%) 466(4; 20%)
18b	$FNH_3^+\cdots F^-$ (C_{3v})	(NH)eq	1.021	0.343	−0.631	−2.340	5.645	1.109	0.9	3192	104(1; 14%) 3459(10; 27%) 3563 (11; 54%)
		(NF)ax	1.428	0.279	−0.249	−0.141	2.687	0.729	0.8	752	748(4; 99%)
		(NF)-PnB	2.039	0.059	−0.004	0.282	1.178	0.458	0.2	498	446(3; 87%) 748(4; 13%)
19	$[FNH_3^+]$ (C_{3v})	NH	1.029	0.338	−0.599	−2.221	6.396	1.190	0.9	3398	3333(7; 33%) 3434(9; 67%)
		NF	1.368	0.332	−0.336	−0.376	5.642	1.109	1.0	1090	1078(1; 99%)
20	NF_6^- (O_h)	NF	1.562	0.210	−0.125	0.157	0.995	0.416	0.6	458	379(4; 20%) 385(6; 61%) 743(13; 13%)
					carbon derivatives						
21	$[CF_4]$ (T_d)	CF	1.321	0.305	−0.502	−0.379	6.204	1.170	1.2	1197	915(6; 16%) 1301(7; 74%)
22a	CF_5^- (D_{3h}) [TS]	(CF)eq	1.331	0.298	−0.486	−0.458	4.535	0.980	1.1	1023	293(4; 20%) 800(10; 18%) 1306(11; 52%)
		(CF)ax	1.699	0.131	−0.086	−0.001	0.554	0.299	0.7	358	514i(1; 60%) 293(4; 39%)
22b	$CF_4\cdots F^-$ (C_{3v})	(CF)ax	1.366	0.274	−0.428	−0.419	4.526	0.979	1.1	1022	612(6; 11%) 901(9; 29%) 1148(10; 58%)
		(CF)[b]	2.813	0.011	0.001	0.048	0.148	0.142	0.1	185	133(3; 99%)
		(CF)eq	1.310	0.313	−0.520	−0.365	6.151	1.164	1.2	1191	901(9; 11%) 1148(10; 12%) 1350 (11; 62%)

DOI: 10.1021/acs.inorgchem.9b02458
Inorg. Chem. 2019, 58, 14777−14789

Table 1. continued

#	molecule (sym.)	bond	r	ρ_b	H_b	$\nabla^2\rho_b$	k^a	BSO	MBO	ω^a	ω^μ(#;ω^a%)
					carbon derivatives						
23a	FCH_3F^- (D_{3h}) [TS]	(CH)eq	1.073	0.310	−0.372	−1.319	5.878	1.135	0.9	3276	3159(10; 33%) 3348(11; 66%)
		(CF)ax	1.826	0.085	−0.031	0.163	0.859	0.383	0.5	445	575i(1; 63%) 371(4; 37%)
23b	$FCH_3\cdots F^-$ (C_{3v})	(CF)ax	1.436	0.206	−0.284	0.125	3.583	0.858	0.8	909	906(4; 98%)
		(CF)-TB	2.558	0.017	0.002	0.079	0.222	0.179	0.0	226	181(3; 98%)
		(CH)eq	1.084	0.300	−0.353	−1.233	5.458	1.088	0.9	3156	3107(10; 33%) 3214(11; 66%)
24	$[FCH_3]$ (C_{3v})	CF	1.389	0.237	−0.346	0.093	5.107	1.048	1.0	1086	1068(1; 97%)
		CH	1.091	0.295	−0.343	−1.190	5.264	1.066	0.9	3100	3045(7; 33%) 3135(9; 67%)
25	CF_6^{2-} (O_h)	CF	1.565	0.180	−0.177	−0.277	0.500	0.282	0.8	340	231(1; 28%) 320(4; 65%)
					boron derivatives						
26	$[BF_3]$ ($D3_h$)	BF	1.315	0.213	−0.171	1.300	7.220	1.274	1.3	1326	891(4; 27%) 1473(5; 71%)
27	$[BF_4^-]$ (T_d)	BF	1.408	0.162	−0.114	0.896	4.107	0.927	1.0	1000	516(3; 10%) 763(6; 16%) 1091(7; 74%)
28	BF_5^{-2} ($D3_h$) [TS]	(BF)eq	1.336	0.200	−0.154	1.182	5.555	1.099	1.0	1163	824(10; 24%) 1391(11; 61%)
		(BF)ax	2.414	0.018	0.000	0.051	0.051	0.078	0.3	112	280i(1; 23%) 81(2; 75%)

[a]Computed at the CCSD(T)/aug-cc-pVTZ level. Bond distances r in Å; electron, energy density, and the Laplacian of the density at the BCP in e/bohr^3, Hartree/bohr^3, and e/bohr^5, respectively. Local stretching force constant k^a in mdyn/Å, bond strength order (BSO), Mayer bond order (MBO), local stretching frequency ω^a in cm^{-1} and the normal-mode frequencies ω^μ related to bond stretching (normal mode number; % of local stretching character). Experimentally observed molecules are given in square brackets. [b]Non-covalent interactions.

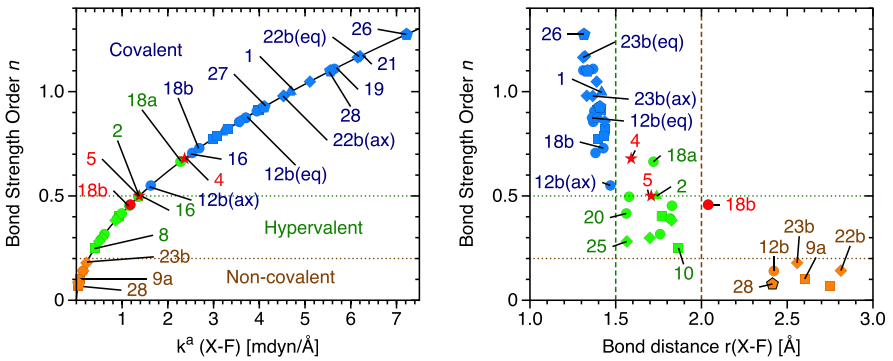

Figure 2. Relationship between the relative bond strength order BSO n and (a) the local stretching force constant k^a(X−F) and (b) the XF bond distances r(X−F) of molecules **1**−**28**; X = F (triangles), O (squares), N (circles), C (diamonds), B (pentagons), Li (stars). Noncovalent interactions are shown in orange, hypervalent bonds in green, covalent bonds in blue, ionic bonds in red.

for OF_4 at the CCSD(T) level. A more rigorous analysis of OF_4 and OF_5^- would require a multireference method capable of providing an accurate description of both dynamic and static electron correlation effects.[85−87]

Dissociation and activation energies, enthalpies, and free energies were calculated utilizing CCSD(T)/aug-cc-pVTZ geometries and harmonic frequencies. To minimize the basis set super position error (BSSE) and to obtain energies closer to the complete basis set limit, single point energies were computed using explicitly correlated coupled cluster CCSD(T)-F12/cc-pVTZ-F12.[88,89] This method and basis set are able to deliver results comparable to those with CCSD(T)/aug-cc-pV5Z.[90]

Besides analyzing the strength of the bonds and the thermodynamic stability, local properties of the electron density,[91] such as the electron density at the bond critical point ρ_b, its Laplacian $\nabla^2\rho_b$, and the total energy density (H_b) obtained from CCSD(T) response density were utilized to access the nature of the bonds. Among these properties, H_b is found to be especially useful to distinguish covalent bonds ($H_b < 0$) from ionic and noncovalent bonds ($H_b \geq 0$).[92]

The charge distribution in molecules **1**−**28** was accessed by calculating atomic charges derived from the Natural Population Analysis (NPA).[93] To obtain a more complete picture of the anisotropic charge distribution, we mapped the electrostatic potential onto the 0.001 e/bohr^3 electron density surface (see Figures S6 and S7). The charge analysis was complemented by the study of electron difference density distributions, comparing the unrelaxed electron density of the fragments in the complex frozen geometry with the relaxed electron density of the complexes (see Figures S7 and S8). Electron density depletion/concentration indicates several phenomena such as polarization, exchange repulsion, and covalent bonding.

All local mode calculations were performed with COLOGNE-2019.[94] CCSD(T)/aug-cc-pVTZ energies, analytic gradients, and Hessians were computed utilizing CFOUR.[95] B-CCD(T) numerical gradients and Hessians were computed with Molpro 15 software.[96] Explicitly correlated CCSD(T)-F12 single point energies were computed with ORCA 4.0.[97] Atomic charges derived from NPA were obtained from NBO 6.0.[98] Correlated electron and energy density distributions were analyzed with Molden2AIM[99] and Multiwfn.[100] Molecular surface graphics were generated in UCSF Chimera.[101]

RESULTS AND DISCUSSION

Table 1 lists bond distances (r), electron density, energy density, and the Laplacian of the electron density at the density critical point of each bond (ρ_b, H_b, and $\nabla^2\rho_b$, respectively). Table 1 also lists all local stretching force constants (k^a), relative bond strength orders (BSO n), Mayer bond orders

DOI: 10.1021/acs.inorgchem.9b02458
Inorg. Chem. 2019, 58, 14777−14789

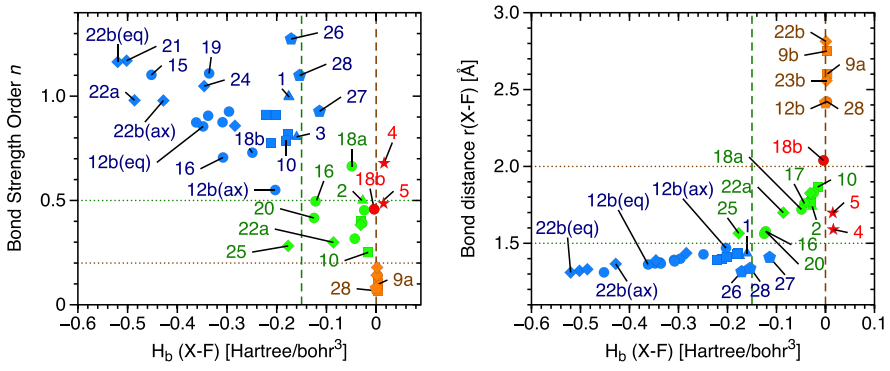

Figure 3. Relationship between (a) the relative bond strength order BSO n and the energy density H_b(X−F) and (b) bond distances r(X−F) and H_b(X−F) for the XF bonds in molecules **1**−**28**; X = F (triangles), O (squares), N (circles), C (diamonds), B (pentagons), Li (stars). Noncovalent interactions are shown in orange, hypervalent bonds in green, classic covalent bonds in blue, ionic bonds in red.

(MBO), local stretching frequencies, and in the last column the normal-mode frequency, the normal mode (m), and the percentage of local stretching character contained in m. The latter are given to provide vibrational spectroscopist information where the stretching bands should be found when recording either infrared or Raman spectra. Molecules experimentally known to exist are given in square brackets in Table 1. NPA atomic charges are given in Figure 1.

The strength of the bonds given by BSO n values, the nature of these bonds given by H_b values, and the charge distribution given by NPA atomic charges were used to assign all X−F (X = Li, B, C, N, O, and F) bonds in molecules **1**−**28** to four different types: covalent, hypervalent, noncovalent, and ionic bonds. As expected from the 3c−4e bond orbital model, MBO values associated with hypervalent bonds are about half the value of comparable 2c−2e covalent bonds (see Table 1). A quantitative ordering of all bonds according to their strength is provided by the relationship between BSO and k^a values given in Figure 2a. The bond strength and bond length relationship (BSBL) is given in Figure 2b. Three out of the four different types of X−F bonds can be easily identified based on their strength or length in the following way: (i) noncovalent bonds are long (r > 2.0 Å) and weak (BSO n < 0.2), (ii) hypervalent bonds have an intermediate strength (0.2 < BSO n) and length (2.0 < r < 1.5 Å), and (iii) covalent bonds are short (r < 1.5 Å) and strong (BSO n > 0.5). The fourth group, comprising ionic bonds, are comparable to the strongest hypervalent bonds but easily identified due to the larger charge separation. For example, in LiF_2^- (**5**), each F atom has a charge close to −1, whereas the electropositive Li has a charge of approximately +1. In hypervalent bonds, the charge at the fluorines involved can vary from −0.263e (**20**) to −0.703e (**23a**).

The BSBL relationship (Figure 2b) shows that bond distances are useful for distinguishing between the different types of bonds, but they cannot be used as a measure of bond strength for a quantitative or even qualitative comparison of bonds of the same type. This is especially noticeable for the hypervalent bonds, where a strong scattering in the BSBL is observed in Figure 2b. The reason for this scattering can be attributed to the different influences equatorial ligands may exert over the hypervalent bond strength and length. For example, the XF hypervalent bond in CF_5^- is shorter but weaker than the one in F_3^-. The shorter bond is a result of the contraction of the covalent radius of X, which is more effective when the electronegativity of X is lower compared to that of F ligands, whereas the weaker bond is due to the increased steric repulsion between ligands. A detailed study of various electronic factors that can lead to scattered or even inverse BSBL relationships was performed by Kraka and co-workers.[102,103]

A long but exceptionally strong hypervalent bond is found for NH_3F_2 (**18**) in its hypervalent TS geometry of D_{3h} symmetry (**18a**). The NF axial bonds of **18a** are stronger than the ones in NF_5 (**16**) and NF_2Cl_3 (BSO (NF)ax: 0.664 (**18a**), 0.496 (**16**), 0.317 (**17**)) but longer than in **16** and of about the same length as in **17**, indicating that the smaller steric repulsion between axial and equatorial ligands in **18a** is not the major factor for the stronger NF bonds. The reason for the stronger bonds is the stabilizing electrostatic interaction between the positively charged equatorial hydrogens and the negative charge at the axial fluorines in **18a**. By deforming from the hypervalent D_{3h} conformation into the C_{3v} ion-pair conformation (**18b**), the 3c−4e FNF bond is lost, but the molecule becomes more stable by forming a strong 2c−2e NF bond and maximizing the electrostatic interaction between hydrogen atoms and fluoride. Ion-pair formation is not observed for **16** and **17**, since they do not benefit from a similarly favorable electrostatic interaction.

The Nature of X−F Bonds. An evaluation of the covalent nature of the four different types of interactions is provided by analyzing the energy density at bond density critical point H_b. According to Cremer and Kraka criteria,[92] a covalent bond is characterized by a negative (stabilizing) H_b value. Figure 3 shows the relationship between BSO values and H_b (Figure 3a) and between bond length r(X−F) and H_b values (Figure 3b). These relationships indicate a somewhat scattered but overall continuous change from weak electrostatic bonds to hypervalent to strong covalent bonds. Weak noncovalent interactions have H_b values close to zero. Hypervalent bonds have intermediate H_b values of 0 < H_b < 0.15 hartree/bohr^3, and covalent bonds tend to have H_b values of >0.15 hartree/bohr^3. There are two major electronic effects responsible for the scattering in the BSO vs H_b relationship. These are (i) high ionic contributions, resulting in relatively strong bonds but with low covalent character, as found for LiF and BF bonds, and (ii) covalent radius contraction of the center atom caused by adding a fluorine substituent followed by increasing steric repulsion between the fluorine ligands, which may lead to weak

DOI: 10.1021/acs.inorgchem.9b02458
Inorg. Chem. 2019, 58, 14777−14789

bonds with relatively high covalent character, as found for the CF bonds of CF_6^{2-} (**25**). It is worth mentioning that the use of the energy density at a single point to characterize the nature of a bond is an approximation,[104,105] which could be improved by integrating the energy density over the interbasin zero-flux surface of electron density, as was recently done by Ananyev and co-workers[106] for the potential energy density analysis. Figure 3b shows a less scattered relationship between bond length and energy density, which is due to the fact that bond lengths (as first-order properties) are less sensitive to variations of H_b (and changes in the electron density in general) than BSO values (derived from a second-order property). For example, the H_b value of the NF equatorial bond of **12b** is 0.16 hartree/bohr^3 lower than that of the axial covalent bond (78% difference); the BSOs of these bonds differ by 0.325 (59%), but their bond lengths differ by just 0.11 Å (8%).

The relationship between bond strength and other properties calculated at the bond critical point $\mathbf{r}_b$, such as the Laplacian of the density $\nabla^2\rho_b$, the potential energy density (V_b), or the kinetic energy density (G_b), are given in the SI (Figures S10−S15). None of them were found to be as insightful and straightforward to interpret as the BSO n versus H_b relationship. Recently, Shaik and co-workers[7] suggested the use of the Laplacian ($\nabla^2\rho_b > 0$) as an indicator of so-called charge-shift bonds. Applying Shaik's criterium to the covalent and hypervalent bonds of the 28 molecules, we find that all OF and FF covalent and all hypervalent bonds (with the CF bonds in **26** as the only exception) are charge-shift bonds. This is in line with their findings[7] showing that hypervalent bonds and bonds between very electronegative elements tend to have charge shift character.

Thermodynamic Stability. Table 2 lists reaction energies (at 0K without zero point vibrational energy corrections), enthalpies, and free energies (at 1 bar and 298.15K) associated with (i) fluoride addition leading to the formation of hypervalent or noncovalent bonded molecules (reactions 1−10); (ii) activation barriers given by the energy difference between hypervalent geometries that are first-order TS and the noncovalent minimum energy geometries (reactions 11−14); and (iii) the energies, enthalpies, and free energies for the dissociation reactions of minimum energy hypervalent molecules into smaller, more stable molecules (reactions 15−20). As one can see, only the addition of F^- to F_2 and to OF_2 (reactions 1 and 3, respectively) lead to thermodynamically stable hypervalent molecules (**2** and **7**) that are not prone to dissociation into smaller fragments. LiF_2^- (**5**) is also thermodynamically stable (reaction 2) but is better described as an ionic system (see NPA charges in Figure 1). Fluoride addition to NF_4^+ leading to NF_5 is thermodynamically viable in the gas phase (reaction 5). However, NF_5 is just a local minimum in the potential energy surface. A more stable product of this reaction is $NF_3 + F_2$ (reaction 17), which is about 40 kcal/mol more stable than NF_5 at 298 K and has a lower free energy of −51.4 kcal/mol at the same temperature (similar results were reported by several authors[20,49,107]). The activation energy associated with the homolytic dissociation of NF_5 into NF_4 and F was estimated by Bettinger and co-workers[20] to be about 16 kcal/mol. Although they could not rule out the existence of hypervalent NF_5, no synthetic strategy has succeeded until now.[5,107] Surprisingly, fluoride addition to the already crowded NF_5 molecules leading to NF_6^- is thermodynamically favorable (reaction 7); however, NF_6^- is unstable with regard to dissociation into smaller molecules

Table 2. Reaction Energies, Enthalpies, and Free Energies[a]

#	reaction	ΔE	ΔE(F12)	ΔH	ΔG
fluoride addition					
1	$F_2 + F^- \rightarrow F_3^-$	−23.8	−23.3	−24.9	−11.9
2	$FLi + F^- \rightarrow FLIF^-$	−69.2	−69.9	−69.4	−61.0
3	$OF_2 + F^- \rightarrow OF_3^-$	−17.6	−16.9	−16.9	−9.5
4	$NF_3 + F^- \rightarrow NF_3\cdots F^-$	−8.3	−8.0	−7.9	−1.8
5	$NF_4^+ + F^- \rightarrow NF_5$	−145.8	−144.4	−145.1	−138.7
6	$FNH_3^+ + F^- \rightarrow FNH_3^+\cdots F^-$	−157.8	−158.0	−158.8	−152.2
7	$NF_5 + F^- \rightarrow NF_6^-$	−27.1	−25.6	−26.1	−16.4
8	$CF_4 + F^- \rightarrow CF_4\cdots F^-$	−7.2	−7.1	−6.9	−0.9
9	$FCH_3 + F^- \rightarrow FCH_3\cdots F^-$	−14.2	−14.0	−13.9	−7.7
10	$CF_4\cdots F^- + F^- \rightarrow CF_6^{2-}$	142.4	144.4	142.1	151.9
activation energies					
11	$NF_3\cdots F^- \rightarrow NF_4^-$(TS)	2.0	2.5	1.4	3.0
12	$FNH_3^+\cdots F^- \rightarrow NH_3F_2$(TS)	4.2	4.7	4.4	6.3
13	$CF_4\cdots F^- \rightarrow CF_5^-$(TS)	20.8	21.4	19.9	22.0
14	$FCH_3\cdots F^- \rightarrow FCH_3F^-$(TS)	13.1	13.3	12.3	14.3
dissociation reactions					
15	$OF_5^- \rightarrow OF_2 + F_2 + F^-$	−0.8	−3.7	−3.9	−20.5
16	$OF_5^- \rightarrow OF_2 + F_3^-$	−24.6	−27.0	−27.1	−36.1
17	$NF_5 \rightarrow NF_3 + F_2$	−37.3	−38.4	−39.7	−51.4
18	$NF_6^- \rightarrow NF_3 + F_2 + F^-$	−10.2	−12.8	−13.6	−35.0
19	$NF_6^- \rightarrow NF_3 + F_3^-$	−34.0	−36.1	−36.8	−50.6
20	$CF_6^{2-} \rightarrow CF_4 + 2F^-$	−134.9	−137.3	−135.2	−151.9

[a]Reaction energies without ZPE computed at CCSD(T)/aug-cc-pVTZ (ΔE) and at CCSD(T)-F12/aVTZ-F12//CCSD(T)/aug-cc-pVTZ (ΔE(F12)). ZPE corrected reaction enthalpies (ΔH(1 bar, 298.15k)) and free energies (ΔG(1 bar, 298.15K)). ZPE, enthalpy, and free energy corrections were computed at the CCSD(T)/aug-cc-pVTZ level and added to ΔE(F12) values. All values are in kcal/mol.

(reaction 18). The existence of NF_6^- under special conditions cannot be discarded either, especially in view of a recent computational simulation,[16] showing that NF_6^- might be spontaneously formed from the oxidation reaction of NF_3 by F_2 under a pressure of 40 GPa. Other hypervalent molecules found to be minima on their potential energy surface but unstable to dissociation are OF_5^- (**10**) and CF_6^{2-} (**20**). Diversely, less crowded hypervalent molecules, NF_4^- (**12a**), NF_3H^- (**13**), NF_2H_3(**18a**), CF_5^-(**22a**), and $CH_3F_2^-$(**23a**), are first-order TSs. The imaginary vibrational mode of all these molecules is the asymmetric stretching of the F−X−F axial bonds, suggesting they gain stability by breaking the 3c−4e bond and forming a covalent 2c−2e XF bond and a noncovalent X···F^- interaction collinear to the axial 2c−2e bond (for X = N in **12b** and **18b**, the noncovalent bond is termed a pnicogen bond (PnB),[108] whereas for X = C in **22b** and **23b**, it is a tetrel bond (TB)[47]). The stabilities gained by the deformation of the hypervalent TS molecules (**12a**, **18a**, **22a**, and **23a**) into noncovalent complexes (**12b**, **18b**, **22b**, and **23b**) are 2.5, 4.7, 21.4, and 13.3 kcal/mol, respectively (reactions 11−14, CCSD(T)-F12 values in Table 2). These noncovalent complexes are formed by two relatively stable closed-shell monomers (e.g., NF_3 and F^-) held together by the electrostatic attraction between the negative charge at the fluoride ion and the positive electrostatic potential formed collinear to the F−X σ-bond of the other monomer (also termed σ hole interaction[109]). A similar mechanism, involving an asymmetric FXF stretching in OF_5^- and CF_6^{2-}, would lead to

DOI: 10.1021/acs.inorgchem.9b02458
Inorg. Chem. 2019, 58, 14777−14789

unstable fragments (OF_4 and CF_5^-), which may explain why these highly crowded hypervalent molecules, unstable to dissociation, are local minima on their potential energy surface.

Analysis of XF Dissociation. To investigate the possible existence of a stable noncovalent minimum $F_2\cdots F^-$ for **2** and $OF_2\cdots F^-$ for **7** and to compare the dissociation curves relative to the XF axial bond of F_3^-, OF_3^-, NF_4^-, CF_5^-, and $CH_3F_2^-$, the XF distance was varied stepwise by small increments. At each step, all other geometric parameters were reoptimized. Figure 4

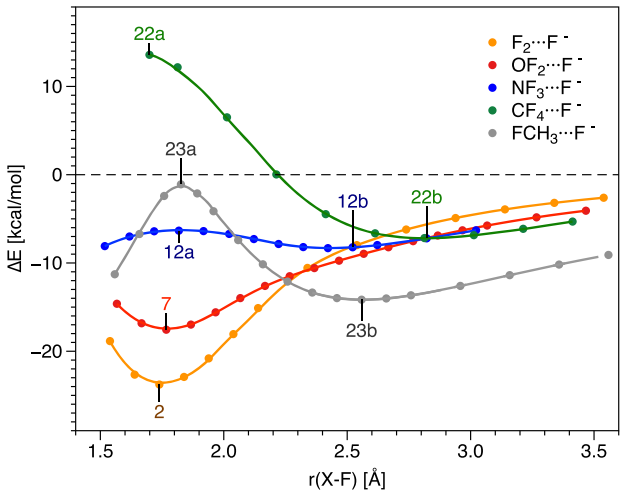

Figure 4. Relationship between the energy in kcal/mol and one X−F (X = F, O, N, and C) axial bond distance in Å relative to the energy of the dissociation products. Calculated at the CCSD(T)/aug-cc-pVTZ level, all parameters but a single axial X−F bond distance were optimized at each point.

shows the X−F dissociation curve of these molecules. The minimum in these potential energy curves corresponds to the hypervalent geometries for **2** and **7** (characterized by symmetric XF axial bonds of about 1.75 Å) and to the noncovalent geometries for **12b**, **22b**, and **23b** (characterized by an X···F$^-$ interaction of 2.4 Å or longer), whereas the maxima in NF_4^-, CF_5^-, and $CH_3F_2^-$ curves correspond to the hypervalent geometries (**12a**, **22a**, and **23a**, respectively). No minima related to $F_2\cdots F^-$ and $OF_2\cdots F^-$ was found for the dissociation curves of F_3^- or OF_3^-.

Due to higher steric crowding effects in **22a**, the CF_5^- curve is the only one where the maximum corresponding to **22a** is not only higher in energy than the noncovalent geometry (**22b**) but is also higher in energy than the dissociation products CF_4 and F$^-$. Another consequence of steric crowding in **22a** is the weaker hypervalent bond (axial CF bond), which is about one-third of the strength of the equatorial 2c−3e bonds (BSO: 0.299 (CF)ax, 0.980 (CF)eq), instead of the expected ratio of about one-half, as found for **7** and **12a**. Substituting axial fluorine ligands with hydrogens lowers the entire energy profile ($CH_3F_2^-$ curve), which indicates that there is not just a decrease in steric effects at **23a** but also a stabilizing electrostatic interaction between the negative charge at the F atoms and the positively charged hydrogens, as observed for NH_3F_2.

The dissociation curve of NF_4^- is considerably flatter than the CF_5^- curve due to the lower steric repulsion, especially at the TS (**12a**). The minima of NF_4^- and CF_5^- corresponding to the noncovalent complexes **12b** and **22b** have similar ΔE and bond strength values (BSO: 0.142 (**12b**), 0.140 (**22b**)) even though the noncovalent N···F$^-$ interaction in **12b** is 0.39 Å shorter than the C···F$^-$ interaction of **22b**. The higher positive electrostatic potential at the σ hole of CF_4, counterbalanced by the larger steric repulsion caused by the three equatorial fluorines, is responsible for the longer noncovalent bond of similar strength. Noteworthy is that the noncovalent interaction in **12b** affects the bond strength of the collinear axial covalent bond more than that of the equatorial bonds (BSO: 0.550 (NF)ax compared to 0.874 (NF)eq). The weakening of a covalent bond collinear to a noncovalent pnicogen bond is usually associated with the electron delocalization from the lone pairs of the pnicogen acceptor (F$^-$ in the present system) into the σ^* antibond orbital of the pnicogen donor (σ^*(NF) orbital in this case).[110,111] However, no significant charge transfer takes place from F$^-$ to NF_3 in **12b** (NPA charge at F$^-$ is $-0.96e$). Therefore, the weakening of the NF axial bond is due to polarization. In short, F$^-$ is attracted by the positive potential at the σ hole of the axial NF bond, and as it gets closer to N, density is pushed from the nitrogen lone pair orbital into the σ^*(NF) orbital of the axial bond, weakening this bond. The low polarity of the OF bond in OF_2 results in a very weak positive electrostatic potential at the σ hole, i.e., to a weak interaction with F$^-$, which is not strong enough to form an $OF_2\cdots F^-$ noncovalent complex.

Relating Energy to Bond Strength. As a bond is broken, the electron density and molecular geometry is rearranged to minimize the energy of the fragments formed. These changes in the electronic and geometric structure (also called deformation energy) have an inherent energetic cost which is not associated with the intrinsic strength of a bond, but which is accounted for by bond dissociation energies.[59] On the other hand, local stretching force constants and associated BSOs measure the rate at which the energy changes when a bond is stretched by an infinitesimally small amount, providing an ideal parameter to measure the intrinsic strength of a bond, free of secondary contributions. A good correlation between BSO values and dissociation energies may be expected only in the case of weakly noncovalently bonded complexes, where electronic and geometric changes are negligible upon dissociation.

Even for the dissociation of strongly bonded systems, the local mode analysis is an invaluable tool, providing a connection between deformation energies and the changes in bond strength of reactants and products of a dissociation. An illustrative example is the comparison between bond dissociation energies and bond strength changes in the hypervalent **2** and the ionic **5** molecules. These molecules have similar bond strengths (BSO: 0.500) but the dissociation energy of F_3^- into F_2 and F$^-$ is about one-third that of LiF_2^- into LiF and F$^-$ (ΔE = 23.3 and 69.9 kcal/mol, respectively). The lower dissociation energy of the former is due to the bigger electronic rearrangement required for the dissociation to take place, i.e., the BSO of the FF bond changes from 0.5 in the reactants (**2**) to 1.0 in the products (**1**), i.e., a difference of 0.5, whereas the BSO of the FLi bond changes by just 0.193 from **5** to **4**. The smaller electronic differences in LiF_2^- and FLi + F$^-$ are also reflected by the smaller variation of the NPA atomic charge of Li and F atoms in **4** and **5**.

Double ionization of **2** leads to the nonhypervalent **3** ion, which has a bent geometry (C_{2v} symmetry) and is isostructural and isoelectronic to OF_2 (**6**). The latter has slightly stronger bonds due to the lower electronegativity of oxygen allowing for more polar bonds.

DOI: 10.1021/acs.inorgchem.9b02458
Inorg. Chem. 2019, 58, 14777−14789

The dissociation energy of OF_3^- into F^- and OF_2 is 6.4 kcal/mol lower than the dissociation energy of F_3^- into F_2 and F^-, which is due to the weaker 3c−4e bonds in **7**. On the basis of the minimal participation of d orbitals in the formation of the hypervalent SF_4 molecule[32,34,36,112] (C_{2v}), one might cogitate the possible stability of the congener OF_4 molecule. However, **9a** (C_{2v} symmetry) is found to be a first-order TS, with an imaginary symmetric stretching mode involving the axial fluorine ligands. The exceedingly long axial OF bonds in this molecule cannot be considered to form a 3c−4e bond due to the insufficient overlap between F and O orbitals. These bonds are better described as weak noncovalent bonds (BSO: 0.102; H_b = 0.004). Several other possible minimum energy geometries were attempted for OF_4, but the only minimum found was the halogen bonded system $F_2\cdots OF_2$.

Unexpectedly, the higher sterically crowded **10** is found to be a minimum energy geometry with C_{4v} symmetry. Different from **9a**, **10** has two sets of 3c−4e bonds formed by the four equatorial fluorines besides the covalent 2c−2e axial OF bond. The existence of these 3c−4e bonds is evidenced by the negative energy density H_b = −0.016, the higher bond strength (BSO = 0.251), and the shorter bond length (1.866 compared to 2.602 Å in **9a**).

Fluoride addition to NF_3 does not lead to a hypervalent molecule (**12a**) but to the noncovalent bonded complexes (**12b**), which is just 2.5 kcal/mol more stable. The electrostatic $N\cdots F^-$ is considerably weaker than the hypervalent bond (BSO: 0.140 compared to 0.392). However, the energetic cost associated with the changes in the electronic/geometric structures of NF_3 necessary for the formation of the 3c−4e bond makes **12a** less favorable than **12b**. A similar analysis can be made to explain why the energetically more stable product of the $NF_4^+ + F^-$ reaction is $F_2 + NF_3$ and not NF_5. The latter product has an additional bond, but due to the weak nature of the 3c−4e bonds, the former product, constituted by two stable molecules with considerably stronger bonds, is 38.4 kcal/mol more stable. In **20**, the stability brought about by the extra NF hypervalent bond surpasses the energy cost associated with changes in **16** structure due to the already weakened bonds of the latter.

For the same reasons as discussed previously for **12b**, the addition of a F^- to CF_4 leads to a noncovalent complex **22b** (the hypervalent geometry (**22a**) is a first-order TS). Comparing **22a** with nitrogen pentafluoride (**16**), the former has a weaker 3c−4e bond due to increased repulsion between axial and equatorial ligands (NPA F(eq): −0.076 (**16**), −0.303 (**22a**)) caused by the higher electronegativity difference between the center atoms and the equatorial ligands. Similar to **10** and **20**, the addition of another fluoride leads to a local minimum in the potential energy surface (**25**). However, due the very weak hypervalent CF bonds (BSO: 0.282 in **25**) this molecule is much less stable than $CF_4 + 2F^-$ (BSO: 1.170 in **21**).

The boron atom in BF_3 (**26**) has a vacant 2p orbital capable of accepting a lone pair of F^- without requiring the formation of a 3c−4e bond. Thus, fluoride addition leading to the nonhypervalent BF_4^- (**27**) is energetically favorable. A 3c−4e bond situation could be realized for BF_5^{-2} if the interaction of the vacant 2p orbital of **26** with the lone pair orbitals of two fluoride atoms at the axial positions was possible. However, repulsion between the fluorides at the axial position and equatorial fluorine ligands (NPA: −0.950e F(ax), −0.521e F(eq)) preclude the formation of hypervalent BF_5^{-2}. Only weak noncovalent interactions are formed between fluorides at the axial position and BF_3 in **28** (BSO (BF)ax 0.078).

CONCLUSIONS AND OUTLOOK

In this work, we analyzed the possible formation of hypervalent first-row molecules held together by 3c−4e bonds and compared the strength and nature of the hypervalent bond in these molecules to suitable 2c−2e covalent bonds and noncovalent bonds, aiming to provide an explanation for their stability or instability. For this purpose, we carried out high accuracy coupled cluster calculations of geometries, reaction energies, and vibrational frequencies, including a comprehensive local mode analysis, combined with the analysis of NPA atomic charges, molecular electrostatic potentials, and an analysis of the electron and energy density at the density critical point of all bonds, for a set of 28 compounds. The following conclusions were reached:

(1) With the exception of F_3^- and OF_3^-, all other hypervalent first-row molecules are either transition state structures (e.g., NF_4^-, NF_3H, NH_3F_2, CF_5^-, and CH_3F_2) or local minima in their potential energy surface (e.g., OF_5^-, NF_5, NF_6^-, NCl_3F_2, and CF_6^{2-}), unstable to dissociation into smaller molecules. Only under special conditions, such as high pressure, may these local minima still be experimentally detectable.[16]

(2) The bond length is useful to distinguish between the different types of interactions. Noncovalent bonds between fluoride and first-row atoms tend to be longer than 2.0 Å, whereas the hypervalent bond lengths are usually between 1.5 and 2.0 Å, and covalent bonds tend to be shorter than 1.5 Å. However, the analysis of the intrinsic bond strength within a group of bonds of the same type requires a parameter being more sensitive to the electronic structure. The BSOs derived from local stretching force constants are the best suited parameters, capable of probing the strength of a bond without breaking it. Noncovalent X−F bonds tend to have BSO values lower than 0.2 and hypervalent bonds between 0.2 and 0.5, the only exception being the NF bond in NF_2H_3, which is stronger due to the electrostatic attraction between positively charged H atoms and negatively charged F atoms. Covalent bonds have BSO values large than 0.5.

(3) Equatorial fluorine substituents cause two main effects: (i) They withdraw charge from the center atom decreasing its effective covalent radius, thus allowing shorter bonds to be formed. (ii) These shorter bonds make axial and equatorial ligands come closer together, increasing steric repulsion, consequently weakening the bonds. For example, the axial CF bonds of CF_5^- are 0.04 Å shorter than FF bonds in F_3^- but are weaker (BSO is lower by 0.2).

(4) Whether the most stable product of a fluoride addition reaction will adopt a hypervalent geometry or a noncovalent complex geometry depends not only on the strength of the new interaction formed but also on the weakening of the other bonds, as a result of the energetic cost associated with the geometric and electronic changes necessary to accommodate the new ligand. Hypervalent 3c−4e bonds are considerably stronger than noncovalent interactions. However, they lead to a substantial weakening of a preexisting 2c−2e bond, which can be accentuated by steric repulsion between axial and equatorial ligands, as observed for CF_5^-, a molecule that gains stability by deforming from the D_{3h} hypervalent conformation into the C_{3v} noncovalent conformation.

(5) Besides steric repulsion, electrostatic attraction can also play a decisive role. For example, while NH_3F_2 gains stability

DOI: 10.1021/acs.inorgchem.9b02458
Inorg. Chem. 2019, 58, 14777−14789

by distorting the hypervalent D_{3h} geometry into the C_{3v} symmetry $FNH_3^+\cdots F^-$ ion-pair geometry, preserving the 2c−2e NF bond, and forming a strong electrostatic interaction, NF_5 and NCl_3F_2 are already stable in their hypervalent geometry, since they cannot form ion pairs with a similarly strong electrostatic interaction.

(6) Even in the noncovalent complexes where charge transfer is small, the formation of an electrostatic interaction between F^- and the positive electrostatic potential at the σ hole of an XF bond results in the weakening of this bond due to polarization effects. This is most noticeable for $NF_3\cdots F^-$, where the BSO value of the axial NF bond decreases by 0.355 (39%) when compared to NF_3, even though no appreciable charge transfer takes place from F^- to NF_3.

On the basis of these findings, we suggest that strategies for the synthesis of stable hypervalent first-row molecules should focus on destabilizing possible noncovalent interactions that can compete with the hypervalent bond formation, e.g., by hosting OF_5^-, NF_5, NF_2H_3, NCl_3F_2, and NF_6^- inside the confined space of a supramolecular structure. Akiba and coworkers[11,14,50] obtained pentacoordinated boron and carbon with symmetric axial interactions that resemble hypervalent molecules by exploiting the limited flexibility imposed by a rigid molecular framework. However, the axial bonds found in these complexes are of about 2.4 Å, being better described as noncovalent interactions; i.e., Akiba complexes are hypercoordinated but not hypervalent. Other strategies such as the use of weaker axial ligands and the formation of other types of nonclassical bonds such as the 3c−2e bond seems to have had some success.[21,113,114]

In this study, it could be shown via a systematic and quantitative way that hypervalent bonds involving first-row atoms are considerably weaker and less covalent than classical 2c−2e bonds. We predict this difference in strength and nature to be significantly lower for second and higher row center atoms due to the more diffuse nature of the valence orbitals of these atoms. Whether the lower bond strength difference between 2c−2e and 3c−4e bonds or the lower steric repulsion among ligands (or maybe both) is responsible for the higher stability of hypervalency in second and higher rows of the periodic table is still an open question, which is currently under investigation.

■ ASSOCIATED CONTENT

Supporting Information

The Supporting Information is available free of charge on the ACS Publications website at DOI: 10.1021/acs.inorgchem.9b02458.

Vertical detachment energies of anions, a comparison between r and k^a values from CCSD(T) and CCSD calculations; T1 diagnostic, T2 largest amplitude, and natural orbitals; comparison between RHF-CCSD(T) and BCCD(T) results; relationships between BSO or r and ρ_b, $\nabla^2\rho_b$, V_b, G_b, G_b/ρ_b, and $|V_b|/G_b$; molecular electrostatic potentials; electron difference densities; geometries and normal vibrational frequencies of all molecules (PDF)

■ AUTHOR INFORMATION

Corresponding Author

*E-mail: fmachado@ita.br.

ORCID

Vytor P. Oliveira: 0000-0002-6614-7625

Elfi Kraka: 0000-0002-9658-5626

Francisco B. C. Machado: 0000-0002-2064-3463

Notes

The authors declare no competing financial interest.

■ ACKNOWLEDGMENTS

We thank Southern Methodist University for providing computational resources. This work has been supported by Brazilian agencies Fundação de Amparo à Pesquisa do Estado de São Paulo (FAPESP) under grants 2017/07707-3 and 2018/13673-7, Conselho Nacional de Desenvolvimento Científico e Tecnoloógico (CNPq) under grants 307052/2016-8 and 404337/2016-3, and the National Science Foundation, Grant CHE 146906.

■ REFERENCES

(1) Dunning, T. H.; Woon, D. E.; Leiding, J.; Chen, L. The first row anomaly and recoupled pair bonding in the halides of the late p-block elements. *Acc. Chem. Res.* **2013**, *46*, 359−368.

(2) Frenking, G., Shaik, S. *The Chemical Bond: Chemical Bonding Across the Periodic Table*; Wiley-VCH: New York, 2014.

(3) Kalescky, R.; Kraka, E.; Cremer, D. Identification of the strongest bonds in chemistry. *J. Phys. Chem. A* **2013**, *117*, 8981−8995.

(4) Schmidt, M. W.; Truong, P. N.; Gordon, M. S. π-Bond strengths in the second and third periods. *J. Am. Chem. Soc.* **1987**, *109*, 5217−5227.

(5) Christe, K. O.; Wilson, W. W.; Schrobilgen, G. J.; Chirakal, R. V.; Olah, G. A. On the existence of pentacoordinated nitrogen. *Inorg. Chem.* **1988**, *27*, 789−790.

(6) Pierrefixe, S. C. A. H.; Fonseca Guerra, C.; Bickelhaupt, F. M. Hypervalent silicon versus carbon: Ball-in-a-box model. *Chem. - Eur. J.* **2008**, *14*, 819−828.

(7) Shaik, S.; Danovich, D.; Braida, B.; Wu, W.; Hiberty, P. C. In *Chem. Bond II. Struct. Bond.*; Michael, D., Mingos, P., Eds.; Springer: Cham, 2015; Chapter 4, pp 169−211.

(8) Lee, D. Y.; Martin, J. C. Compounds of pentacoordinate (10-B-5) and hexacoordinate (12-B-6) hypervalent boron. *J. Am. Chem. Soc.* **1984**, *106*, 5745−5746.

(9) Kudo, H. Observation of hypervalent CLi_6 by Knudsen-effusion mass spectrometry. *Nature* **1992**, *355*, 432−434.

(10) Ault, B. S.; Andrews, L. Infrared and Raman spectra of the M +F3- ion pairs and their mixed chlorine-fluorine counterparts in solid argon. *Inorg. Chem.* **1977**, *16*, 2024−2028.

(11) Kikuchi, Y.; Ishii, M.; Akiba, K.-y.; Nakai, H. Discovery of hexacoordinate hypervalent carbon compounds: Density functional study. *Chem. Phys. Lett.* **2008**, *460*, 37−41.

(12) Malischewski, M.; Seppelt, K. Crystal structure determination of the pentagonal-pyramidal hexamethylbenzene dication $C_6(CH_3)_6^{2+}$. *Angew. Chem., Int. Ed.* **2017**, *56*, 368−370.

(13) Goesten, M. G.; Hoffmann, R.; Bickelhaupt, F. M.; Hensen, E. J. M. Eight-coordinate fluoride in a silicate double-four-ring. *Proc. Natl. Acad. Sci. U. S. A.* **2017**, *114*, 828−833.

(14) Yamaguchi, T.; Yamamoto, Y.; Kinoshita, D.; Akiba, K. Y.; Zhang, Y.; Reed, C. A.; Hashizume, D.; Iwasaki, F. Synthesis and structure of a hexacoordinate carbon compound. *J. Am. Chem. Soc.* **2008**, *130*, 6894−6895.

(15) Hirano, Y.; Kojima, S.; Yamamoto, Y. A Hypervalent Pentacoordinate Boron Compound with an N-B-N Three-Center Four-Electron Bond. *J. Org. Chem.* **2011**, *76*, 2123−2131.

(16) Kurzydłowski, D.; Zaleski-Ejgierd, P. Hexacoordinated nitrogen(V) stabilized by high pressure. *Sci. Rep.* **2016**, *6*, 36049.

(17) Pei, Y.; An, W.; Ito, K.; Schleyer, P. v. R.; Zeng, X. C. Planar pentacoordinate carbon in CAl_5^+: A global minimum. *J. Am. Chem. Soc.* **2008**, *130*, 10394−10400.

DOI: 10.1021/acs.inorgchem.9b02458
Inorg. Chem. 2019, 58, 14777−14789

(18) Gao, Y.; Shao, N.; Zhou, R.; Zhang, G.; Zeng, X. C. [CTi_7^{2+}]: Heptacoordinate carbon motif? *J. Phys. Chem. Lett.* **2012**, *3*, 2264−2268.
(19) Guo, J.-C.; Ren, G.-M.; Miao, C.-Q.; Tian, W.-J.; Wu, Y.-B.; Wang, X. $CBe_5H_n^{n4}$ (n = 25): Hydrogen-stabilized CBe_5 pentagons containing planar or quasi-planar pentacoordinate carbons. *J. Phys. Chem. A* **2015**, *119*, 13101−13106.
(20) Bettinger, H. F.; Schleyer, P. v. R.; Schaefer, H. F. NF_5viable or not? *J. Am. Chem. Soc.* **1998**, *120*, 11439−11448.
(21) Pierrefixe, S. C. A. H.; van Stralen, S. J. M.; van Stralen, J. N. P.; Fonseca Guerra, C.; Bickelhaupt, F. M. Hypervalent carbon atom: Freezing the Sn2 transition state. *Angew. Chem., Int. Ed.* **2009**, *48*, 6469−6471.
(22) Landrum, G. A.; Goldberg, N.; Hoffmann, R. Bonding in the trihalides (X_3^-), mixed trihalides (X_2Y^-) and hydrogen bihalides (X_2H^-). The connection between hypervalent, electron-rich three-center, donoracceptor and strong hydrogen bonding. *J. Chem. Soc., Dalton Trans.* **1997**, 3605−3613.
(23) Crabtree, R. H. Hypervalency, secondary bonding and hydrogen bonding: siblings under the skin. *Chem. Soc. Rev.* **2017**, *46*, 1720−1729.
(24) Yannacone, S.; Oliveira, V.; Verma, N.; Kraka, E. A continuum from halogen bonds to covalent bonds: Where do λ3 iodanes fit? *Inorganics* **2019**, *7*, 47.
(25) Wolters, L. P.; Bickelhaupt, F. M. Halogen bonding versus hydrogen bonding: A molecular orbital perspective. *ChemistryOpen* **2012**, *1*, 96−105.
(26) Setiawan, D.; Sethio, D.; Cremer, D.; Kraka, E. From strong to weak NF bonds: on the design of a new class of fluorinating agents. *Phys. Chem. Chem. Phys.* **2018**, *20*, 23913−23927.
(27) Wang, Y.; Li, F.; Li, Y.; Chen, Z. Semi-metallic Be_5C_2 monolayer global minimum with quasi-planar pentacoordinate carbons and negative Poisson's ratio. *Nat. Commun.* **2016**, *7*, 11488.
(28) Yang, L.-M.; Ganz, E.; Chen, Z.; Wang, Z.-X.; Schleyer, P. V. R. Four decades of the chemistry of planar hypercoordinate compounds. *Angew. Chem., Int. Ed.* **2015**, *54*, 9468−9501.
(29) Fernández, I.; Frenking, G.; Uggerud, E. The interplay between steric and electronic effects in Sn2 reactions. *Chem. - Eur. J.* **2009**, *15*, 2166−2175.
(30) Wolfe, S.; Mitchell, D. J.; Schlegel, H. B. Theoretical studies of SN2 transition states. 1. Geometries. *J. Am. Chem. Soc.* **1981**, *103*, 7692−7694.
(31) Hamlin, T. A.; Swart, M.; Bickelhaupt, F. M. Nucleophilic substitution (Sn2): Dependence on nucleophile, leaving group, central atom, substituents, and solvent. *ChemPhysChem* **2018**, *19*, 1248.
(32) Musher, J. I. The chemistry of hypervalent molecules. *Angew. Chem., Int. Ed. Engl.* **1969**, *8*, 54−68.
(33) Lewis, G. N. The atom and the molecule. *J. Am. Chem. Soc.* **1916**, *38*, 762−785.
(34) Mitchell, K. A. R. Use of outer d orbitals in bonding. *Chem. Rev.* **1969**, *69*, 157−178.
(35) Coulson, C. A. d-Electrons and molecular bonding. *Nature* **1969**, *221*, 1106−1110.
(36) Magnusson, E. Hypercoordinate molecules of second-row elements: d functions or d orbitals? *J. Am. Chem. Soc.* **1990**, *112*, 7940−7951.
(37) Reed, A. E.; Schleyer, P. v. R. Chemical bonding in hypervalent molecules. The dominance of ionic bonding and negative hyperconjugation over d-orbital participation. *J. Am. Chem. Soc.* **1990**, *112*, 1434−1445.
(38) Braïda, B.; Hiberty, P. C. The essential role of charge-shift bonding in hypervalent prototype XeF_2. *Nat. Chem.* **2013**, *5*, 417−422.
(39) Pimentel, G. C. The bonding of trihalide and bifluoride ions by the molecular orbital method. *J. Chem. Phys.* **1951**, *19*, 446−448.
(40) Rundle, R. E. Electron deficient compounds. II. Relative energies of "half-bonds. *J. Chem. Phys.* **1949**, *17*, 671−675.
(41) Schmokel, M. S.; Cenedese, S.; Overgaard, J.; Jorgensen, M. R. V.; Chen, Y.-S.; Gatti, C.; Stalke, D.; Iversen, B. B. Testing the Concept of Hypervalency: Charge Density Analysis of K_2SO_4. *Inorg. Chem.* **2012**, *51*, 8607.
(42) Fugel, M.; Malaspina, L. A.; Pal, R.; Thomas, S. P.; Shi, M. W.; Spackman, M. A.; Sugimoto, K.; Grabowsky, S. Revisiting a Historical Concept by Using Quantum Crystallography: Are Phosphate, Sulfate and Perchlorate Anions Hypervalent? *Chem. - Eur. J.* **2019**, *25*, 6523−6532.
(43) Munzarová, M. L.; Hoffmann, R. Electron-rich three-center bonding: Role of s,p Interactions across the p-block. *J. Am. Chem. Soc.* **2002**, *124*, 4787−4795.
(44) Braida, B.; Ribeyre, T.; Hiberty, P. C. A valence bond model for electron-rich hypervalent species: Application to SF_n (n = 1, 2, 4), PF_5, and.ClF_3. *Chem. - Eur. J.* **2014**, *20*, 9643−9649.
(45) Woon, D. E.; Dunning, T. H. Hypervalency and recoupled pair bonding in the p-block elements. *Comput. Theor. Chem.* **2011**, *963*, 7−12.
(46) Dunning, T.; Woon, D.; Xu, L.; Takeshita, T.; Lindquist, B.; Leiding, J. In *Annual Reports in Computational Chemistry*; Dixon, D. A., Ed.; Elsevier: New York, 2016; Vol. *12*; pp 81−113.
(47) Sethio, D.; Oliveira, V.; Kraka, E. Quantitative assessment of tetrel bonding utilizing vibrational spectroscopy. *Molecules* **2018**, *23*, 2763.
(48) Sakata, K. Force constant decomposition for penta-coordinated $XH_3Cl_2^-$ (X = C, Si, Ge) structures. *J. Comput. Chem.* **2018**, *39*, 1544−1550.
(49) Grant, D. J.; Wang, T.-H.; Vasiliu, M.; Dixon, D. A.; Christe, K. O. F^+ and F^- affinities of simple N_xF_y and O_xF_y compounds. *Inorg. Chem.* **2011**, *50*, 1914−1925.
(50) Nakai, H.; Okoshi, M.; Atsumi, T.; Kikuchi, Y.; Akiba, K.-y. Theoretical design of hexacoordinate hypervalent carbon compounds by analyzing substituent effects. *Bull. Chem. Soc. Jpn.* **2011**, *84*, 505−510.
(51) Sidorkin, V. F.; Doronina, E. P.; Belogolova, E. F. A new approach to the design of neutral 10-C-5 trigonal-bipyramidal carbon compounds: A π-electron cap effect. *Chem. - Eur. J.* **2013**, *19*, 10302−10311.
(52) Durrant, M. C. A quantitative definition of hypervalency. *Chem. Sci.* **2015**, *6*, 6614−6623.
(53) Hirano, Y.; Kojima, S.; Yamamoto, Y. A hypervalent pentacoordinate boron compound with an N-B-N three-center four-electron bond. *J. Org. Chem.* **2011**, *76*, 2123−2131.
(54) Rocha, M. V.; Smits, N. W.; Wolters, L. P.; de Cózar, A.; Fonseca Guerra, C.; Ramalho, T. C.; Bickelhaupt, F. M. Asymmetric identity S_N2 transition states: Nucleophilic substitution at α-substituted carbon and silicon centers. *Int. J. Mass Spectrom.* **2017**, *413*, 85−91.
(55) Marchaj, M.; Freza, S.; Skurski, P. Why are $SiX_5^-$and (GeX_5^-X = F, Cl) stable but not and CF_5^- CCl_5^- ? *J. Phys. Chem. A* **2012**, *116*, 1966−1973.
(56) Nakanishi, W.; Nakamoto, T.; Hayashi, S.; Sasamori, T.; Tokitoh, N. Atoms-in-molecules analysis of extended hypervalent five-center, six-electron (5c-6e) C_2Z_2O interactions at the 1,8,9-positions of anthraquinone and 9-methoxyanthracene systems. *Chem. - Eur. J.* **2007**, *13*, 255−268.
(57) Harcourt, R. D. Valence bond representations for Sn2 reactions. *J. Mol. Struct.: THEOCHEM* **1988**, *165*, 329−340.
(58) Zou, W.; Cremer, D. C_2in a box: Determining its intrinsic bond strength for the $X^1\Sigma_g^+$ ground state. *Chem. - Eur. J.* **2016**, *22*, 4087−4089.
(59) Cremer, D.; Kraka, E. From molecular vibrations to bonding, chemical reactions, and reaction mechanism. *Curr. Org. Chem.* **2010**, *14*, 1524−1560.
(60) Oliveira, V.; Cremer, D. Transition from metal-ligand bonding to halogen bonding involving a metal as halogen acceptor a study of Cu, Ag, Au, Pt, and Hg complexes. *Chem. Phys. Lett.* **2017**, *681*, 56−63.

DOI: 10.1021/acs.inorgchem.9b02458
Inorg. Chem. 2019, 58, 14777−14789

(61) Wilson, E. B.; Decius, J. C.; Cross, P. C. *Molecular Vibrations. The Theory of Infrared and Raman Vibrational Spectra*; McGraw-Hill: New York, 1955.
(62) Wilson, E. B., Jr A Method of Obtaining the Expanded Secular Equation for the Vibration Frequencies of a Molecule. *J. Chem. Phys.* **1939**, *7*, 1047−1952.
(63) Konkoli, Z.; Cremer, D. A new way of analyzing vibrational spectra I. Derivation of adiabatic internal modes. *Int. J. Quantum Chem.* **1998**, *67*, 1−11.
(64) Kraka, E.; Cremer, D. Dieter Cremer's contribution to the field of theoretical chemistry. *Int. J. Quantum Chem.* **2019**, *119*, No. e25849.
(65) Oliveira, V.; Cremer, D.; Kraka, E. The many facets of chalcogen bonding: Described by vibrational spectroscopy. *J. Phys. Chem. A* **2017**, *121*, 6845−6862.
(66) Von Ragué Schleyer, P.; Martin, J. C. Hypervalent compounds. *Chem. Eng. News* **1984**, *62*, 4.
(67) Raghavachari, K.; Trucks, G. W.; Pople, J. A.; Head-Gordon, M. A fifth-order perturbation comparison of electron correlation theories. *Chem. Phys. Lett.* **1989**, *157*, 479−483.
(68) Woon, D.; Dunning, T. J. Gaussian basis sets for use in correlated molecular calculations. IV. Calculation of static electrical response properties. *J. Chem. Phys.* **1994**, *100*, 2975−2988.
(69) Dunning, T. Gaussian basis sets for use in correlated molecular calculations. I. The atoms boron through neon and hydrogen. *J. Chem. Phys.* **1989**, *90*, 1007−1023.
(70) Woon, D.; Dunning, T. Gaussian basis sets for use in correlated molecular calculations. III. The atoms aluminum through argon. *J. Chem. Phys.* **1993**, *98*, 1358−1371.
(71) Unal, A.; Bozkaya, U. Anionic water pentamer and hexamer clusters: An extensive study of structures and energetics. *J. Chem. Phys.* **2018**, *148*, 124307.
(72) Cremer, D. Møller-Plesset perturbation theory: From small molecule methods to methods for thousands of atoms. *Wiley Interdiscip. Rev. Comput. Mol. Sci.* **2011**, *1*, 509−530.
(73) Howard, J. C.; Tschumper, G. S. Benchmark Structures and Harmonic Vibrational Frequencies Near the CCSD(T) Complete Basis Set Limit for Small Water Clusters: $(H_2O)_{n=2,3,4,5,6}$. *J. Chem. Theory Comput.* **2015**, *11*, 2126−2136.
(74) Harding, M. E.; Metzroth, T.; Gauss, J.; Auer, A. A. Parallel calculation of CCSD and CCSD(T) analytic first and second derivatives. *J. Chem. Theory Comput.* **2008**, *4*, 64−74.
(75) Zou, W.; Kalescky, R.; Kraka, E.; Cremer, D. Relating normal vibrational modes to local vibrational modes with the help of an adiabatic connection scheme. *J. Chem. Phys.* **2012**, *137*, 084114.
(76) Cremer, D.; Kraka, E. Generalization of the Tolman electronic parameter: The metal-ligand electronic parameter and the intrinsic strength of the metal-ligand bond. *Dalt. Trans.* **2017**, *46*, 8323−8338.
(77) Setiawan, D.; Kraka, E.; Cremer, D. Description of pnicogen bonding with the help of vibrational spectroscopy - The missing link between theory and experiment. *Chem. Phys. Lett.* **2014**, *614*, 136−142.
(78) Kraka, E.; Larsson, J. A.; Cremer, D. In *Computational Spectroscopy*; Grunenberg, J., Ed.; Wiley: New York, 2010; pp 105−149.
(79) Badger, R. M. A Relation Between Internuclear Distances and Bond Force Constants. *J. Chem. Phys.* **1934**, *2*, 128−132.
(80) Badger, R. M. The Relation Between Internuclear Distances and the Force Constants of Diatomic Molecules. *Phys. Rev.* **1935**, *48*, 284−285.
(81) Badger, R. M. The Relation Between the Internuclear Distances and Force Constants of Molecules and Its Application to Polyatomic Molecules. *J. Chem. Phys.* **1935**, *3*, 710−715.
(82) Lee, T. J. Comparison of the T1 and D1 diagnostics for electronic structure theory: A new definition for the open-shell D11 diagnostic. *Chem. Phys. Lett.* **2003**, *372*, 362−367.
(83) Valeev, E. F.; Botee, H. M.; Schaefer, H. F. Is F_3^+viable? A high-level a*b initio* comparison of F_3^+ and Cl_3^+. *J. Chem. Phys.* **1998**, *109*, 1772−1780.
(84) Chiles, R. A.; Dykstra, C. E. An electron pair operator approach to coupled cluster wave functions. Application to He_2, Be_2, and Mg_2 and comparison with CEPA methods. *J. Chem. Phys.* **1981**, *74*, 4544−4556.
(85) Bozkaya, U. Efficient Implementation of the Second-Order Quasidegenerate Perturbation Theory with Density-Fitting and Cholesky Decomposition Approximations: Is It Possible To Use Hartree-Fock Orbitals for a Multiconfigurational Perturbation Theory? *J. Chem. Theory Comput.* **2019**, *15*, 4415−4429.
(86) Lyakh, D. I.; Musial, M.; Lotrich, V. F.; Bartlett, R. J. Multireference Nature of Chemistry: The Coupled-Cluster View. *Chem. Rev.* **2012**, *112*, 182−243.
(87) Lischka, H.; Nachtigallova, D.; Aquino, A. J. A.; Szalay, P. G.; Plasser, F.; Machado, F. B. C.; Barbatti, M. Multireference Approaches for Excited States of Molecules. *Chem. Rev.* **2018**, *118*, 7293−7361.
(88) Adler, T. B.; Knizia, G.; Werner, H.-j. A simple and efficient CCSD(T)-F12 approximation. *J. Chem. Phys.* **2007**, *127*, 221106.
(89) Peterson, K. A.; Adler, T. B.; Werner, H. J. Systematically convergent basis sets for explicitly correlated wavefunctions: The atoms H, He, B-Ne, and Al-Ar. *J. Chem. Phys.* **2008**, *128*, 084102.
(90) Bischoff, F. A.; Wolfsegger, S.; Tew, D. P.; Klopper, W. Assessment of basis sets for F12 explicitly-correlated molecular electronic-structure methods. *Mol. Phys.* **2009**, *107*, 963−975.
(91) Bader, R. F. W. A quantum theory of molecular structure and its applications. *Chem. Rev.* **1991**, *91*, 893−928.
(92) Cremer, D.; Kraka, E. A description of the chemical bond in terms of local properties of electron density and energy. *Croat. Chem. Acta* **1984**, *57*, 1259−1281.
(93) Reed, A. E.; Weinstock, R. B.; Weinhold, F. Natural population analysis. *J. Chem. Phys.* **1985**, *83*, 735−746.
(94) Kraka, E.; Zou, W.; Filatov, M.; Grafenstein, J.; Izotov, D.; Gauss, J.; He, Y.; Wu, A.; Konkoli, Z.; Polo, V.; Olsson, L.; He, Z.; Cremer, D. *COLOGNE2019*; Computational and Theoretical Chemistry Group (CATCO), Southern Methodist University: Dallas, TX, 2019. See: http://www.smu.edu/catco (accessed Jun 10, 2019).
(95) Stanton, J. F.; Gauss, J.; Harding, M. E.; Szalay, P. G. *CFOUR*; University of Texas at Austin: Austin, TX; Universität Mainz: Mainz, Germany, 2010. See http://www.cfour.de (accessed Jul 31, 2017).
(96) Werner, H. J.; Knowles, P. J.; Knizia, G.; Manby, F. R.; Schütz, M.; Celani, P.; Korona, T.; Lindh, R.; Mitrushenkov, A.; Rauhut, G.; et al. *MOLPRO*, Version 2015.1; Cardiff University: Cardiff, U. K.; Universität Stuttgart: Stuttgart, Germany, 2010. See http://www.molpro.net (accessed Jun 10, 2019).
(97) Neese, F. Software update: the ORCA program system, version 4.0. *Wiley Interdiscip. Rev. Comput. Mol. Sci.* **2018**, *8*, No. e1327.
(98) Glendening, E. D.; Landis, C. R.; Weinhold, F. NBO 6.0: Natural bond orbital analysis program. *J. Comput. Chem.* **2013**, *34*, 1429−1437.
(99) Zou, W.; Nori-Shargh, D.; Boggs, J. E. On the covalent character of rare gas bonding interactions: A new kind of weak interaction. *J. Phys. Chem. A* **2013**, *117*, 207−212.
(100) Lu, T.; Chen, F. Multiwfn: A multifunctional wavefunction analyzer. *J. Comput. Chem.* **2012**, *33*, 580−592.
(101) Pettersen, E. F.; Goddard, T. D.; Huang, C. C.; Couch, G. S.; Greenblatt, D. M.; Meng, E. C.; Ferrin, T. E. UCSF Chimera?A visualization system for exploratory research and analysis. *J. Comput. Chem.* **2004**, *25*, 1605−1612.
(102) Kraka, E.; Setiawan, D.; Cremer, D. Re-evaluation of the bond length-bond strength rule: The stronger bond is not always the shorter bond. *J. Comput. Chem.* **2016**, *37*, 130−142.
(103) Setiawan, D.; Kraka, E.; Cremer, D. Hidden bond anomalies: The peculiar case of the fluorinated amine chalcogenides. *J. Phys. Chem. A* **2015**, *119*, 9541−9556.
(104) Kraka, E.; Cremer, D. *Theoretical Models of Chemical Bonding. The Concept of the Chemical Bond*; Maksic, Z. B., Ed.; Springer Verlag: Heidelberg, 1990; Vol. *2*; p 453.

DOI: 10.1021/acs.inorgchem.9b02458
Inorg. Chem. 2019, 58, 14777−14789

(105) Kraka, E.; Cremer, D. Description of chemical reactions in terms of the properties of the electron density. *J. Mol. Struct.: THEOCHEM* **1992**, *255*, 189−206.
(106) Ananyev, I. V.; Karnoukhova, V. A.; Dmitrienko, A. O.; Lyssenko, K. A. Toward a rigorous definition of a strength of any interaction between bader's atomic basins. *J. Phys. Chem. A* **2017**, *121*, 4517−4522.
(107) Lewars, E. G. *Model Marvels*; Springer: Dordrecht, The Netherlands, 2008; Chapter 4, pp 53−65.
(108) Oliveira, V.; Kraka, E. Systematic coupled cluster study of noncovalent interactions involving halogens, chalcogens, and pnicogens. *J. Phys. Chem. A* **2017**, *121*, 9544−9556.
(109) Politzer, P.; Murray, J. S. σ hole interactions: Perspectives and misconceptions. *Crystals* **2017**, *7*, 212.
(110) Scheiner, S. The pnicogen bond: Its relation to hydrogen, halogen, and other noncovalent bonds. *Acc. Chem. Res.* **2013**, *46*, 280−288.
(111) Oliveira, V.; Kraka, E. Systematic coupled cluster study of noncovalent interactions involving halogens, chalcogens, and pnicogens. *J. Phys. Chem. A* **2017**, *121*, 9544−9556.
(112) Cooper, D. L.; Cunningham, T. P.; Gerratt, J.; Karadakov, P. B.; Raimondi, M. Chemical bonding to hypercoordinate second-row atoms: D orbital participation versus democracy. *J. Am. Chem. Soc.* **1994**, *116*, 4414−4426.
(113) McKee, W. C.; Agarwal, J.; Schaefer, H. F.; Schleyer, P. v. R. Covalent hypercoordination: Can carbon bind five methyl ligands? *Angew. Chem., Int. Ed.* **2014**, *53*, 7875−7878.
(114) Pierrefixe, S. C. A. H.; Poater, J.; Im, C.; Bickelhaupt, F. M. Hypervalent versus nonhypervalent carbon in noble-gas complexes. *Chem. - Eur. J.* **2008**, *14*, 6901−6911.

DOI: 10.1021/acs.inorgchem.9b02458
Inorg. Chem. 2019, 58, 14777−14789